

Supporting material for
Force-sensitive autoinhibition of the von Willebrand factor mediated
by inter-domain interactions

Camilo Aponte-Santamaría[†], Volker Huck[‡], Sandra Posch[§], Agnieszka K. Bronowska[†], Sandra Grässle[‡],
Maria A. Brehm[¶], Tobias Obser[¶], Reinhard Schneppenheim[¶], Peter Hinterdorfer[§], Stefan W. Schneider[‡],
Carsten Baldauf^{||}, and Frauke Gräter[†]

[†]Molecular Biomechanics Group, Heidelberg Institute for Theoretical Studies, Heidelberg, Germany

[‡]Experimental Dermatology, Medical Faculty Mannheim, Heidelberg University, Mannheim, Germany

[§]Department of Applied Experimental Biophysics, Institute of Biophysics, Johannes Kepler University, Linz, Austria

[¶]Department of Pediatric Hematology and Oncology, University Medical Center Hamburg-Eppendorf, Hamburg, Germany

^{||}Theory Department, Fritz-Haber-Institut der Max-Planck-Gesellschaft, Berlin, Germany

Supporting figures

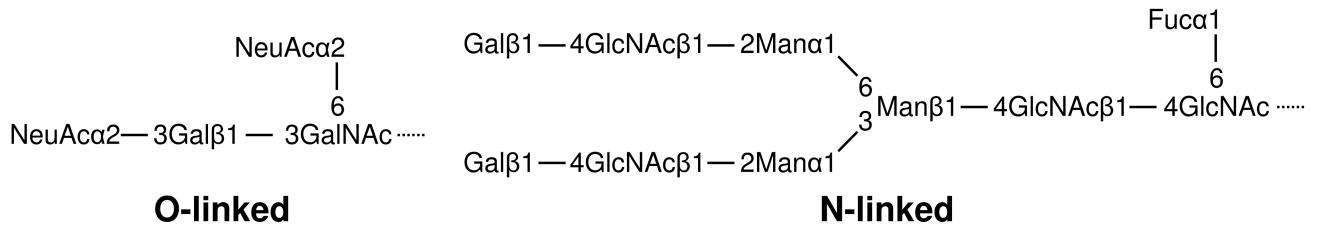


Figure S1. O-linked (left) and N-linked (right) sugars used in the molecular dynamics (MD) simulations of the von Willebrand factor (VWF) A1 and A2 domains. They were attached to the side chains of the glycosylated residues highlighted in Fig. 1A in the main text. They are the two most predominant sugars bound to VWF, accounting for 62.5 % of the O-linked and 59.9 % of the N-linked sugars.

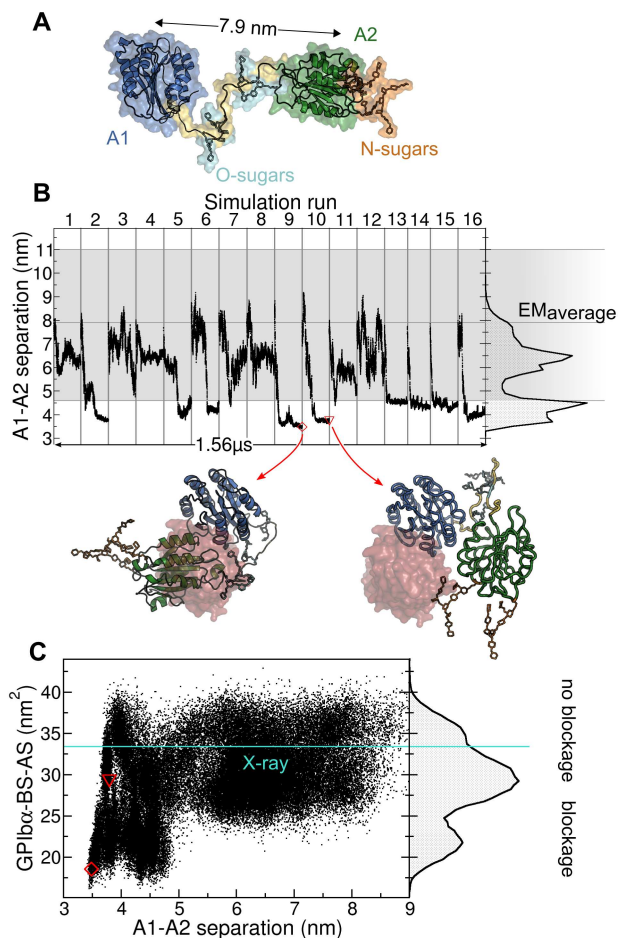


Figure S2. Blockage of the GPIb α binding site in the von Willebrand factor (VWF) revealed by molecular dynamics (MD) simulations of the VWF-A1A2 fragment, including the inter-domain linker. **A.** Typical starting conformation used in the MD simulations (protein as cartoon and surface, and sugars as sticks). Residues 1269 to 1670 of the human VWF were considered. The A1 (blue) and A2 (green) domains are connected by a 30 residue linker (yellow). Four O-linked sugars (O-sugars, cyan) are located at the linker and two N-linked sugars (N-sugars, orange) at the A2 domain. The initial domain-domain center of mass (A1-A2) separation is indicated with the black arrow. Multiple inter-domain starting orientations were considered. **B.** A1-A2 separation along the concatenated MD simulation time. Gray lines separate individual MD runs. Right plot displays the normalized histogram of the A1-A2 separation. The range of separations observed by electron microscopy (1) is depicted in gray (average, minimum and maximum highlighted with the horizontal lines). Conformations at the bottom show examples, with the two domains in contact (cartoon) contrasted to the region occupied by GPIb α when it binds to A1 (red surface), taken at the instants marked with the open red symbols. **C.** GPIb α binding site accessible surface (GPIb α -BS-AS) as a function of the A1-A2 separation (main panel) and its normalized histogram (right plot). Reduced GPIb α -BS-AS values correspond to blockage of the GPIb α binding site. The GPIb α -BS-AS derived from the VWF A1-GPIb α complex X-ray structure (2) is indicated by the cyan line. The open symbols correspond to the conformations shown at the bottom of B.

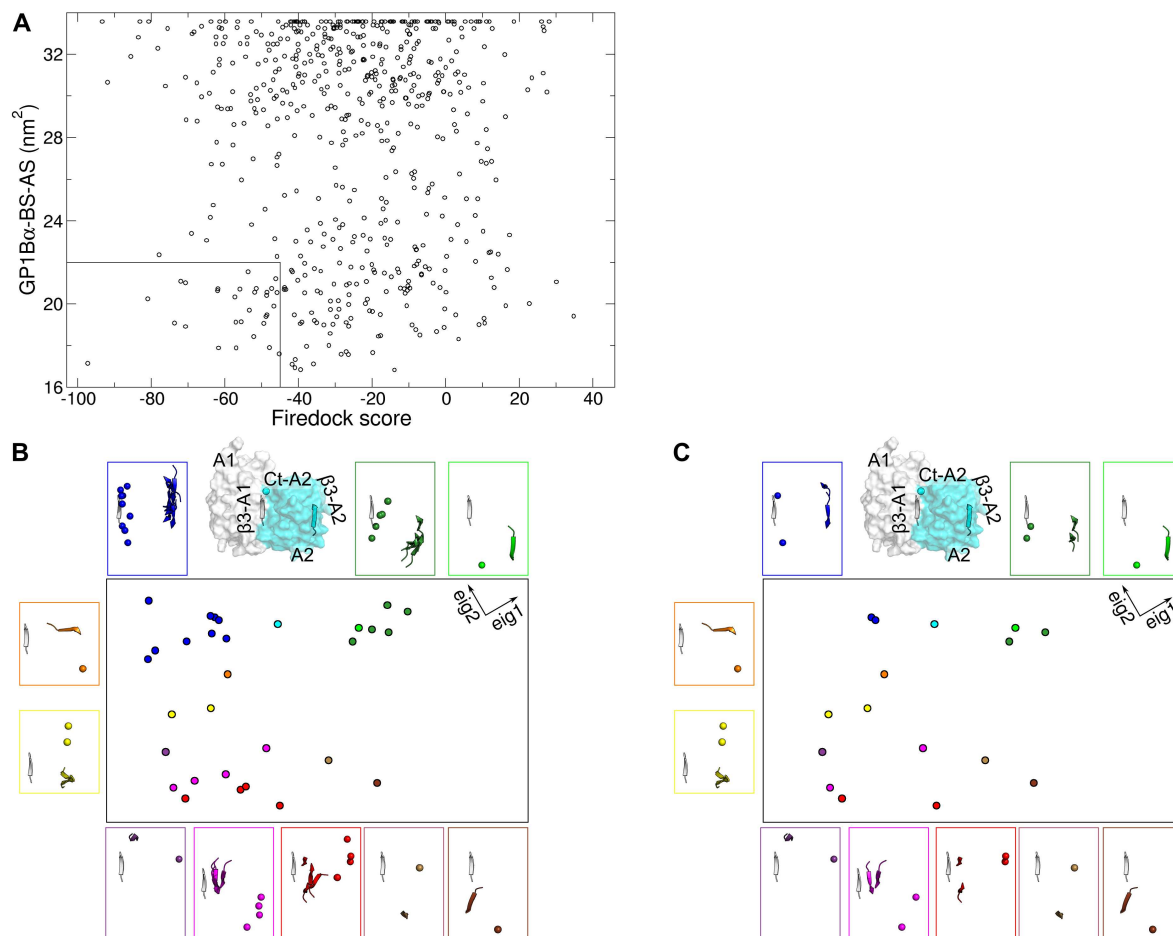


Figure S3. Docking of von Willebrand factor (VWF) A2 domain to the VWF A1 domain, resulting in blockage of the GP1B α binding site. **A.** A set of conformations with the A1 and A2 domains of the VWF in contact with each other was generated by using Patchdock and refined using Firedock. For the resulting conformations, the GP1B α binding site accessible surface (GP1B α -BS-AS) is plotted as a function of the Firedock ranking score. The conformations presenting both substantial blockage and high Firedock scores (laying in the square at the lower left corner) were selected. **B.** Conformations were clustered based on their RMSD yielding 11 groups (different colors). The orientations belonging to each group are displayed in the colored boxes (with the β 3 strand in cartoon and the C-terminus of the A2 domain in sphere representation, and the A1 domain in white and the A2 domain in color). The protein surface is also depicted for the group colored with cyan. A principal component analysis (PCA) considering this set of conformations yielded two principal collective vectors eig1 and eig2 (which together accounted for 68% of the inter-domain orientational changes). Conformations were projected onto the 2-dimensional (2D) space constituted by these two vectors in the black square (each circle represents one conformation), confirming the clustering between conformations. **C.** From each group the two (or one in the case of only one) conformations with highest Firedock ranking scores were selected as the starting positions for the MD simulations presented in Fig. 2A in the main text. Their orientations and projections (onto the 2D PCA space created by all the conformations) are shown here (with the same format as in B). See further details of the docking procedure in the supporting text. In B and C projections are in arbitrary units.

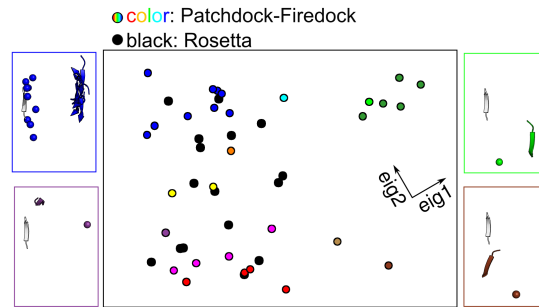


Figure S4. Comparison between Patchdock-Firedock and Rosetta molecular docking. Projections of the conformations of the von Willebrand factor (VWF) A1 and A2 domains, in contact and blocking the GPIb α binding site, predicted by Patchdock and Firedock (color) compared to the ones predicted by Rosetta (black). Projections were done onto 2-dimensional Patchdock and Firedock principal component space (presented in Fig. S3), with each circle representing one conformation. Overlap between projections indicate similar predictions by the two docking methodologies. To facilitate the comparison, the conformations associated to some projections are illustrated in the colored squares (with the β 3 strands in cartoon and the C-terminus of the VWF A2 domain in sphere representation, and with VWF A1 in white and VWF A2 in the same color as in the projections). Projections are in arbitrary units.

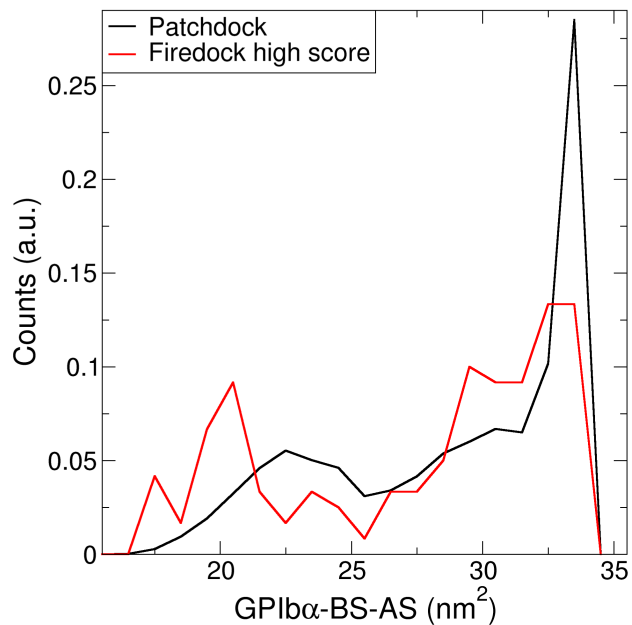


Figure S5. Distribution of the GPIb α binding site accessible surface (GPIb α -BS-AS) for all possible poses predicted by Patchdock and for the ones with high Firedock score.

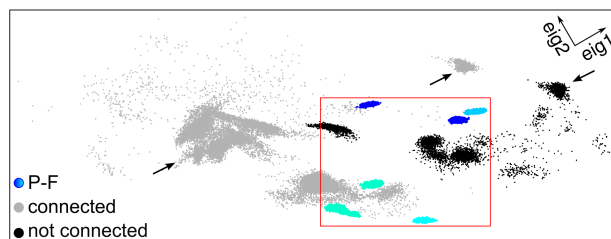


Figure S6. Comparison between orientations extracted from different simulations of the von Willebrand factor (VWF) A1 and A2 domains, in contact and blocking the GP1B α binding site. Projections onto the 2-dimensional Patchdock and Firedock (P-F) principal component space (presented in Fig. S3), with each circle representing one conformation. Projections of the refined docking-MD set (presented in Fig. 2 of the main text) are shown in color. Projections from trajectories starting from connected and separated domains are displayed in gray (set from Fig. S2), and from not connected and separated domains in black (set from Fig. 1). The red square indicates the extent of the refined docking-MD data set, with the A2 domain situated directly in front of the β 3 strand of the A1 domain, which was also covered by the other two data sets. The arrows point to regions populated only in the simulations starting with separated domains. Projections in arbitrary units.

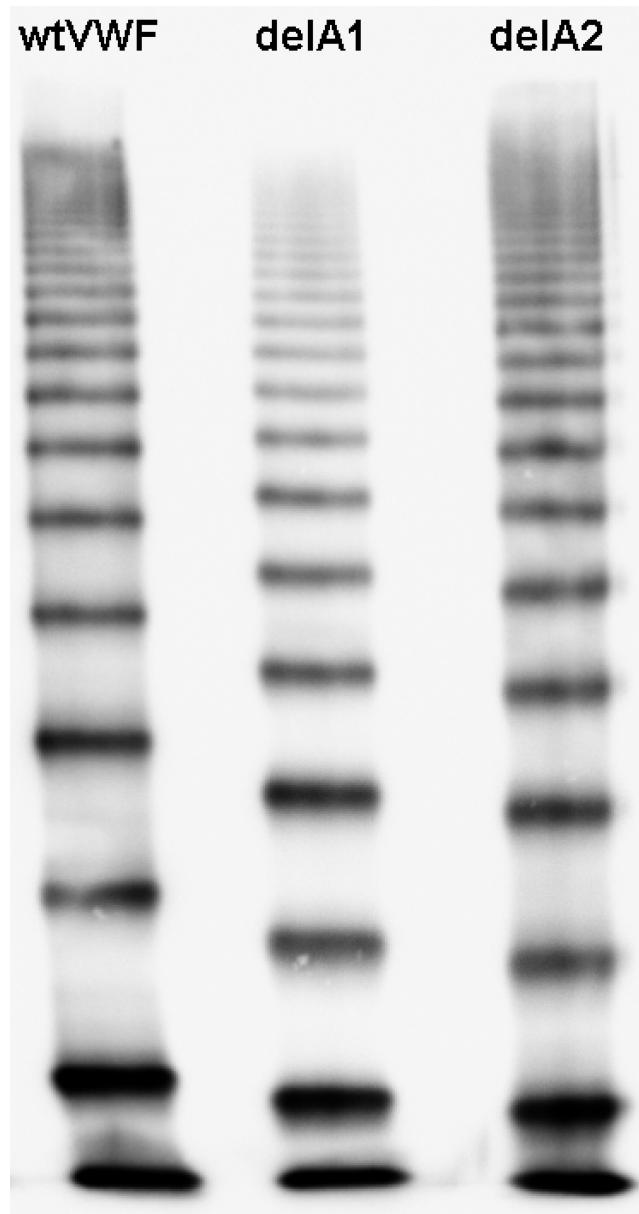


Figure S7. Multimer analysis of recombinant VWF. Multimer analysis of recombinant wild-type VWF (wtVWF) and deletion mutants lacking either the A1 (delA1) or the A2 (delA2) domain was performed by SDS agarose electrophoresis gels and immunoblotting onto nitrocellulose membrane with luminescent visualisation.

Supporting video S1

Comparison of flow through microfluidic channels, perfused with wild-type VWF (upper channel) versus VWF with the A2 domain deleted (lower channel). (Minute 1) Shear is maintained constant at 500 s^{-1} . Here, rolling of single platelets is observed for both proteins. (Minute 2-4) Shear is kept fixed at 2500 s^{-1} . Large rolling aggregates, formed by platelets and VWF, are observed for the VWF lacking the A2 domain (lower channel), while only reversibly formed platelet-decorated VWF fibers, which stayed attached to the channel surface are observed for wild-type VWF (upper channel). (Minute 5-end of the movie) Shear is retained at a value of 4000 s^{-1} . Large aggregates are formed for both proteins. Frames were taken at a frequency of 2 frames per second. Time is indicated in seconds the first minute and in minutes after. The white bar corresponds to $100\text{ }\mu\text{m}$. Platelets and VWF are shown in white.

Supporting text

1 Molecular dynamics (MD) simulations

1.1 Equilibrium MD simulations of not connected von Willebrand factor (VWF) A1 and A2 domains

The starting atomic positions of the A1 and A2 domains were taken from their X-ray structures (PDB ids. 1AUQ (3) and 3GXB (4), respectively). The two domains were initially separated by distances (between center of masses) varying from 6.1 nm to 8.6 nm. The N-linked sugars considered for the simulations are shown in Fig. S1. They account for 59.9 % of the N-linked (5) sugars bound to VWF. Their atomic coordinates were obtained with the Glycoprotein web server GLYCAM-Web (www.glycam.org) (6). They were attached to Asn1515 and to Asn1574, in the A2 domain. For the attachment, the sugars were aligned to the side chain of the residues, using PyMOL (7) and the *g_confrms* tool of the GROMACS package (8–10), ensuring that there were no steric clashes neither with other sugars nor with the protein. Internal disulfide bonds observed in the X-ray structures (3, 4) were imposed between the cysteine pairs Cys1272-Cys1458 in the A1 domain and Cys1669-Cys1670 in the A2 domain. The two domains were solvated by ~ 121000 water molecules, and sodium and chloride ions ($\sim 150\text{ mM}$ concentration) in a dodecahedron box. Additional sodium ions were added to maintain the system electrically neutral. An energy minimization step and a simulation of 1 ns, equilibrating the solvent with all the heavy atoms of the complex harmonically restrained, preceded the production runs. 17 independent 100 ns MD simulations, with different starting inter-domain orientations, were carried out, yielding $1.7\text{ }\mu\text{s}$ concatenated simulation time. See Section 1.4 below for the used force field, and algorithms and parameters employed during the energy minimization, solvent equilibration, system neutralization, and MD simulations.

In addition, 16 MD simulations of 100 ns each ($1.6\text{ }\mu\text{s}$ concatenated time), starting with the two domains in contact forming a complex were carried out. The starting structures of the complex

were obtained by docking the structures of A1 and A2 using Patchdock (11) and refined using Fire-dock (12). See details of the docking procedure in Section 4 and selection of starting conformations in Fig. S3. Same simulation parameters as above were used, except for a smaller simulation box containing 24000 to 55000 water molecules and a longer solvent equilibration of 10 ns (with the N-linked sugars also free to move).

1.2 Equilibrium MD simulations of connected VWF A1 and A2 domains

MD simulations of the VWF-A1A2 fragment (residues 1269 to 1670 of the VWF sequence), consisting of the A1 and A2 domains connected by a 30 amino acid linker, were carried out. Starting structures of the domains were the same as in the simulations of the unconnected A1 and A2 domains (Section 1.1), but here, the two domains were separated by a distance (between center of masses) of 7.9 nm, corresponding to the average separation observed in electron microscopy (EM) images (1). In addition to the N-linked sugars attached to the A2 domain, the O-linked sugar accounting for 62.5 % of the VWF O-glycome (13) (Fig. S1) was appended to the linker at residues Thr1468, Thr1477, Ser1486 and Thr1487. Atomic coordinates for the O-linked sugars were obtained with the Glycoprotein web server GLYCAM-Web (www.glycam.org) (6), and the same attachment procedure was applied as for the N-linked sugars in Section 1.1. To generate the initial conformation of the linker, a 50 ns equilibrium MD simulation, starting from a completely stretched, fully solvated and O-linked glycosylated linker, was carried out. From this simulation, a conformation with an end to end distance of 6.0 nm (in accordance to the EM estimates (1)) was selected. Next, the domains were placed at different orientations, and connected by the resulting 6 nm linker. 16 independent MD simulations, with lengths from 82 ns to 100 ns (for $\sim 1.56\mu\text{s}$ concatenated simulation time), were carried out. They were preceded by the following equilibration steps. First, the fragment was placed in a cubic box containing approximately 53000 water molecules and sodium and chloride ions at $\sim 150\text{mM}$ concentration, with an excess of sodium ions to keep the system electrically neutral. Second, the system was energy minimized. Third, the solvent was equilibrated during 1 ns, with the protein harmonically restrained. Fourth, the linker was equilibrated during 10 ns, by releasing its restraints, but still maintaining the A1 and A2 domains harmonically fixed. Fifth, to allow full rotation, the fragment was accommodated in a larger dodecahedron box, which contained approximately 135000 water molecules. Sixth, the solvent was equilibrated in the new box during 500 ps, with the fragment harmonically restrained. Finally, restraints on the fragment were released. The used force field, and simulation algorithms and parameters are described in detail in Section 1.4 below.

1.3 Force-probe MD simulations

Force-probe simulations of not connected A1 and A2 domains forming a complex were performed by exerting an external harmonic force F_1 on the N-terminus of the A1 domain and F_2 on the C-terminus of the A2 domain. Harmonic springs (with elastic constants $K = 500\text{kJmol}^{-1}\text{nm}^{-2}$) were attached to these termini, and were moved away from each other along the x axis at a constant

pulling velocity, V , of 0.2 m/s. Harmonic forces (acting along the x -axis) were computed as

$$F_i(t) = -K [x_i(t) - x_i(0) - V_i t], \quad i = 1, 2. \quad (1)$$

Here, $x_i(t)$ is the terminus x -coordinate ($i = 1$ for the A1 N-terminus and $i = 2$ for the A2 C-terminus) at time t . The harmonic spring attached to the A1 N-terminus was moved at velocity $V_1 = -V/2$ and the one attached to the A2 C-terminus at velocity $V_2 = V/2$.

Simulations were started from 17 different starting conformations. One conformation was extracted from one of the equilibrium simulations of the two domains showing spontaneous binding (run number 8 in Fig. 1C of main text). The remaining 16 corresponded to a representative conformations extracted from the equilibrium MD simulations of the A1 and A2 domains forming a complex. For each run, the complex was aligned along the x axis and centered in a cubic box of water solvent and sodium and chloride ions at ~ 150 mM concentration. The box dimensions were approximately the diameter of the complex, adding 11.5 nm in the x -axis and 1.5 nm in the y - and z -axis, to provide enough space to accommodate the stretched fragments of the protein. Extra sodium ions were added to neutralize the net charge of the protein. The system was energy minimized and the solvent was equilibrated for 1 ns (with the protein harmonically restrained).

Simulations were continued until the complex dissociated. For two cases, the springs reached the box walls in the x -axis and the domains were still in complex. For these two cases, force probe MD simulations were continued without increasing the simulation box size, after deleting the unfolded C-terminal part of the A2 domain (20 residues in one and 21 residues the other case). It was ensured that the deleted portion was almost fully stretched and that the tensile force was nearly zero at the moment of deletion, thereby causing a minimum effect on the elastic constant of the pulling springs. The remaining part of the complex was re-centered in the box, energy minimized, solvent equilibrated for 500 ps (with the protein harmonically restrained), and subjected to harmonic forces, starting with the same forces on the termini as at the moment of deletion.

The used force field, and the algorithms and parameters for energy minimization, solvent equilibration, system neutralization, and MD simulations are presented in Section 1.4 below.

1.4 Force field and MD simulation parameters

In addition to water molecules, sodium and chloride ions (at 150 mM concentration) and an excess of sodium ions to keep the system electrically neutral were always added to the system. All simulations were carried out with the GROMACS package (8–10, 14) (4.5.5 version). The Amber99sb-ildn* force field (15–17) was used for the protein, GLYCAM06 parameters for the sugars (18), the TIP3P model (19) for the water molecules, and parameters determined by Joung *et al.* (20) for the ions. Energy minimizations were carried out with the steepest descent algorithm. Solvent equilibration simulations were carried out with the protein heavy atoms harmonically restrained (harmonic force constant of $1000 \text{ kJmol}^{-1} \text{ nm}^{-2}$). Constraints were imposed over all bonds by using the LINCS algorithm (21) and virtual interaction-sites were added to take into account fast angular motions

involving hydrogen atoms (22). For the water molecules, both bond lengths and angles were constrained by means the Settle algorithm (23). The use of these bond and angular constraint algorithms allowed to integrate Newtonian equations of motion by using of the leap frog algorithm (24) at discrete time steps of 4 fs. Electrostatic and short-range non-bonded interactions were considered. The particle-mesh Ewald method (25, 26) was used to compute the electrostatic interactions, while a Lennard Jones potential modeled the short-range interactions (only considered within a cut-off of 10 Å). The system was simulated under constant temperature and pressure (NPT) conditions. The temperature was maintained constant at 300 K and pressure to 1 bar, by coupling the system to a velocity-rescaling thermostat (27, 28) (coupling constant $\tau = 0.5$ ps) together with a Parrinello-Rahman barostat (29) (coupling constant $\tau = 5.0$ ps).

2 GPIb α binding site accessible surface (GPIb α -BS-AS)

The GPIb α binding site was constituted by the residues in the A1 domain which were found at a distance smaller than 6 Å from the GPIb α protein, in the X-ray structure of the VWF A1-GPIb α complex (2) (PDB code 1SQ0). The joined surface of the A1 and A2 domains of the VWF (either in contact or separated) was obtained by rolling a sphere with a radius of 5.0 Å on the protein-surface atoms, as described by the Connolly algorithm (30). From that surface, the part corresponding to the GPIb α binding site (in the A1 domain) exposed to the surface was selected, and its area was the GPIb α -BS-AS.

3 Principal component analysis

Principal component analysis (PCA) (31), consisting in the calculation and diagonalization of the covariance matrix of the atomic coordinates, was employed to monitor the inter-domain orientations. The backbone atoms of the $\beta 3$ strands (of both domains) and the $\beta 6$ strand of the A2 domain were considered for the PCA calculation. The structures were fitted by superimposing the A1 domain to its initial structure. The structures predicted by molecular docking with Patchdock and Firedock (section 4) were used to generate the diagonalized covariance matrix. Two major PCA eigenvectors constituted 68 % of the possible orientational motions of the A2 domain around the A1 domain. MD trajectories were projected on the 2-dimensional space constituted by these two PCA vectors, to reflect the different orientations adopted by the A2 domain with respect to the A1 domain during the simulations.

4 Molecular docking

Molecular docking was used to generate conformations of the A1 and A2 domains forming a complex. The X-ray structures of the A1 domain (PDB id 1AUQ) (3) and the A2 domain (PDB id 3GXB) (4) were docked using Patchdock (11). Blind docking, without any constraints, was performed, thus implying no prior bias towards particular conformations. Redundant poses with an

RMSD smaller than 6 Å were clustered yielding an initial set of 11020 possible conformations. They were sorted according to their inter-domain shape complementarity, and 606 conformations were selected for further refinement: the 300 with highest shape complementarity and other 306, selecting one conformation every 35 in the sorted set. Refinement was carried out using Firedock (12). For the resulting conformations, the amount of blockage was quantified by computing the GPIb α binding site accessible surface (GPIb α -BS-AS) on the A1 domain. This quantity was plotted as a function of the Firedock ranking score (an empirical estimate of the binding free energy), and the conformations presenting both substantial blockage and high Firedock scores (more negative values) were considered for further calculations (Fig. S3A). In practice, the ones among the 20% with lowest GPIb α -BS-AS values and also among the 20% with lowest Firedock scores were selected. The blocking highly-ranked selected conformations were also clustered according to their RMSD (clustering cutoff of 1.0 nm), yielding 11 representative groups (Fig. S3B). From each group the two (or one in the case of only one) conformations with highest Firedock scores were selected as representative of each group (Fig. S3C), and used as the starting positions for the MD refinement simulations of not connected and bound A1 and A2 domains (see Section 1.1).

Putative poses of the complex were also predicted independently using the RosettaDock protein-protein docking method (32). Its framework relies on identification of low-energy conformations of a protein-protein interaction near a given starting configuration by optimizing the rigid-body orientation and side-chain conformations. 25 initial geometries were provided, which differed in the relative orientation of the two domains. RosettaDock generated 1000 independent structures, and the coordinates for the best model (per starting conformation) were selected.

Molecular docking predicted highly ranked Firedock poses having effect on the GPIb α accessible surface area as well as poses having little effect (Fig. S3A). This was not surprising, given the limitations of docking to predict the distribution of structures occurring naturally. We tested if there was any gain in considering high-score poses instead of any random pose. To this end, we compared the GPIb α -BS-AS of the 11020 poses of the complex predicted by Patchdock, which covered all possible random orientations of the two domains when they are bound to each other, with the values obtained for the 20% best ranked Firedock poses (Fig. S5). The GPIb α -BS-AS for the Patchdock set did not show any preference for either the blocked (low GPIb α -BS-AS) or the non-blocked (high GPIb α -BS-AS) state. In contrast, by selecting only the poses with high Firedock score (which have high shape complementary and favourable protein-protein interactions between the two domains), there is an increment in the number of structures presenting blockage compared to that number in the Patchdock, the random, set, almost three fold for poses with GPIb α -BS-AS < 22 nm² (compare black with red in Fig. S5 for low GPIb α -BS-AS). This suggests that a structure in the blocked state is favoured over any random structure, due to its high inter-domain shape complementary and favorable protein-protein interactions. This further supports that A2 targets the GPIb α binding site in A1. Furthermore, it justifies our selection criterion, to only structures with both with high blockage and high Firedock score.

5 Cloning, expression and purification of VWF constructs

Plasmid constructs

The cDNAs coding for either the full-length human VWF, the A1 domain (residues 1230 to 1462) and the A2 domain (residues 1494 to 1672), the latter two with 6x His-tag, were cloned into the mammalian expression vector pcDNA3 (33). Δ A1-VWF and Δ A2-VWF mutants were obtained by deleting either the A1 domain (residues 1260 to 1479) or the A2 domain (residues 1493 to 1673) from the full-length cDNA, by site-directed mutagenesis employing the QuickChange kit (Stratagene). All primers are available upon request. The plasmids were sequenced and used to transform Top10 supercompetent cells (Invitrogen). Plasmid purification was performed using the Endofree Plasmid Maxi Kit (QIAGEN).

Cell culture and expression of VWF constructs in HEK293 EBNA cells

HEK293 EBNA cells were cultured in Dulbecco Modified Eagle Medium (DMEM, Invitrogen) with 10% [v/v] fetal bovine serum (Invitrogen) and 1% penicillin/streptomycin at 37 °C and 5% CO₂. HEK293 EBNA cells were transfected with the VWF vectors using Lipofectamine 2000 (Invitrogen) according to the manufacturer's instructions, and a stable cell-line was selected with G418. The recombinant expression of VWF variants was performed in OPTIPRO-SFM (Invitrogen) for 72 hours.

Protein purification

The His-tagged VWF domain constructs were purified employing the His-Pur Ni-NTA Resin (Thermo Scientific) according to the manufacturer's instruction for purification of His-tagged proteins using a gravity-flow column.

Multimer analysis

Multimer analysis was performed as previously described (34–36). In brief, VWF multimers of recombinant VWF samples were separated by SDS-agarose electrophoresis, transferred onto a nitrocellulose membrane and detected with anti-human VWF antibody-HRP linked (DAKO) and visualised by luminescence.

6 Atomic force microscopy (AFM)

Chemicals

All chemicals were used in the highest available purity. 3-Aminopropyltriethoxy silane (APTES; SigmaAldrich, Vienna, Austria) was distilled at low pressure and stored under argon in sealed crimp vials over silica gel (to avoid polymerization) at a temperature of -20 °C. MilliQ (Millipore, USA) purified water was used for all aqueous solutions. Triethylamine (TEA, SigmaAldrich, Vienna,

Austria) was stored under argon in the dark to avoid amine oxidation. Chloroform was purchased from J.T. Baker (Griesheim, Germany), argon and N₂ from Linde Gas GmbH (Stadl-Paura, Austria). The heterobifunctional crosslinker maleimide-PEG-NHS was provided by Hermann Gruber, Johannes Kepler University (Linz, Austria) and used as described in (37). Ethylenediaminetetraacetic acid (EDTA) was purchased from VWR International (Vienna, Austria), Hepes and NiCl₂ from Merck (Darmstadt Germany), and tris(2-carboxyethyl)phosphine (TCEP) hydrochloride from Molecular Probes, Invitrogen (Vienna, Austria). Disulfide-tris-NTA was generously provided by Prof. Robert Tampé, Biocenter of the Goethe University (Frankfurt am Main, Germany). Mica sheets were bought from Christine Groepl, Electron Microscopy (Tulln, Austria).

AFM cantilevers

For single molecule force spectroscopy (SMFS) experiments non-conductive silicon nitride MSCT tips (Bruker Corporation, USA, D-cantilever, with a 30 pNnm⁻¹ nominal spring constant) were used. The actual spring constant was determined according to Hutter *et al.* (38) using the thermal noise method.

Buffers

The used buffers were TBS buffer (50 mM Tris, and 150 mM NaCl at pH 7.5 adjusted with NaOH), and the Hepes buffer (1 M Hepes at pH 7.5 or pH 9.6, respectively adjusted with NaOH).

Tip and sample chemistry

Amino-functionalization: Commercial MSCT cantilevers were washed with chloroform (3×5 min incubation) and dried in a gentle nitrogen gas stream prior further treatment. For surface functionalization mica sheets were cleaved immediately before further use. The APTES functionalization was performed as described previously (39): A desiccator (51) was flooded with argon gas to remove air and moisture. Then two small plastic trays (e.g. the lids of Eppendorf reaction vials) were placed inside the desiccator, 30 ml of APTES and 10ml of triethylamine were separately pipetted into two trays. The AFM tips and the mica sheets were placed nearby on a clean inert surface (e.g. Teflon) and the desiccator was closed. After 120 min of incubation, APTES and triethylamine were removed, the desiccator was again flooded with argon gas for 5 min, and the tips were left inside for two days in order to cure the APTES coating.

Coupling of maleimide-PEG-NHS: The linker coupling was performed as described (37): In brief, APTES functionalized AFM tips or APTES coated mica sheets (samples) were incubated in 0.5 ml (tips) and in 1.5 ml (mica sheets) of a 1 mg/ml solution of maleimide-PEG-NHS in chloroform containing 0.5% (v/v) of TEA as catalyst for two hours. Subsequently, the tips and mica sheets were rinsed in chloroform (3×5 min) and dried in a gentle stream of nitrogen gas.

Coupling of His6-tagged VWF A1 or A2 domains: The cantilevers and mica sheets were placed on Parafilm in a polystyrene Petri dish and a mixture of 100 μl disulfide-tris-NTA (1 mM in MilliQ

water), 2 μl EDTA (100 mM, pH 7.5 in MilliQ water), 5 μl Hepes (1 M, pH 7.5 in MilliQ water), 2.5 μl TCEP hydrochloride (100 mM in MilliQ water), 2.5 μl Hepes (1 M, pH 9.6 in MilliQ water) was pipetted onto the tips and mica sheets and incubated for two hours. Subsequently tips and mica sheets were washed in TBS buffer (3x5 min) before they were placed on Parafilm in a polystyrene Petri dish and pre-loaded with 50 μl TBS buffer containing 2 μl of 5 mM NiCl_2 to obtain a final concentration of 200 μM NiCl_2 (pH 7.5) for 5 minutes. Subsequently 100 μl of the His6-tagged protein were mixed with 4 μl of NiCl_2 (5 mM) and again incubated for 2 hours. Finally tips and mica sheets were washed 3 times for 5 minutes in TBS and stored in TBS at a temperature of 4 °C until further use.

Single Molecule Force Spectroscopy

SMFS measurements were performed on a scanning probe microscope (Pico SPM Plus setup, Agilent, USA) under near physiological conditions. VWF A1 domains were C-terminally coupled to the AFM tip and VWF A2 domains were C-terminally immobilized to the mica sheet surface. Force distance cycles (FDC) were acquired at room temperature in TBS buffer by approaching the AFM tip towards the surface, followed by its retraction. Specific interactions were discerned from nonspecific adhesion by a differing approach and retraction force signal. To have an unbiased choice of binding events, FDC displaying a characteristic worm-like-chain-type force signal, as well as FDC not showing such behavior, were included for further analysis. To prove the specificity of the interactions between the A1 and the A2 domain, control experiments were carried out either in the presence of 0.1 mg/ml soluble A2 domains or by replacing either the A1 or the A2 domain by VWF A3 domain. The position of the tip relative to the surface was changed every 200 FDC, to statistically avoid position dependent artifacts. Four tips (each functionalized either with the VWF A1 domain or the VWF A3 domain) were utilized. At least 1000 FDC were recorded for each of the tips at a pulling speed of 600 nm/s. The number of binding events in relation to the whole number of acquired FDC was computed. It should be noted that unbinding events occur sequentially, as it is very unlikely to have identical elongations for two unbinding events simultaneously (40). In fact, multiple binding events were observed only in rare cases (at the most two bindings and in less than 4%), and they were not considered for further analysis. The elongation L of the pulled construct (A1, A2, coating molecules, and linkers) was monitored during the experiments. Its expectation value (EV) was computed from his probability distribution as $EV = \sum_i P_i L_i$, where P_i is the probability of occurrence of an elongation L_i .

7 Microfluidic experiments

For distinct shear rate application, air-pressure driven microfluidic channels (BioFlux, USA) were coated with 50 $\mu\text{g}/\text{mL}$ recombinant wild-type VWF over night at 37 °C. For preparation of the perfusion media, blood was collected from healthy volunteers using sodium citrated blood vacuum collection tubes. The study was conducted in conformity to the Declaration of Helsinki (41) and

to The International Conference on Harmonization of Technical Requirements for Registration of Pharmaceuticals for Human Use (ICH) Guidelines, available at <http://www.ich.org>, accessed in October 2010. It was approved by the Ethics Committee of the Medical Faculty Mannheim, Heidelberg University (Mannheim, Germany). Appropriate informed consent was obtained from all subjects. To functionally characterize the impact of the VWF A2 domain on the GPIIb α -VWF A1 domain interaction, wild-type VWF coated microfluidic channels were mounted onto an inverted fluorescence microscope (Zeiss Axio Observer Z.1, Zeiss AG, Oberkochen, Germany) and perfused as previously published (42), with the wild-type VWF, VWF with the A2 domain deleted, or VWF with the A1 domain deleted. Briefly, washed platelets were used in a concentration of 200000 per μ l stained with Celltrace calcein-green (Invitrogen, USA). This solution was supplemented with 45% washed haematocrit in HEPES buffered ringer solution. Focusing on the shear dependent ability to form platelet binding strings, the plasmatic VWF fraction was replaced with 10 μ g/mL recombinant VWF, either wild-type or with the A1 or the A2 domain deleted. Live cell fluorescence videos were taken at two frames per second at various shear rates in the range of 500 s^{-1} to 4000 s^{-1} (with a nominal shear rate precision of 36 s^{-1}). For image analysis we used the ZEN package (Zeiss AG, Jena, Germany) and the open-source software ImageJ (V. 1.46r, National Institute of Health, USA).

Supporting material references

- [1] Zhou, Y.-F., E. T. Eng, N. Nishida, C. Lu, T. Walz, and T. A. Springer, 2011. A pH-regulated dimeric bouquet in the structure of von Willebrand factor. *EMBO J* 30:4098–4111.
- [2] Dumas, J. J., R. Kumar, T. McDonagh, F. Sullivan, M. L. Stahl, W. S. Somers, and L. Mosyak, 2004. Crystal structure of the wild-type von Willebrand factor A1-glycoprotein Ib α complex reveals conformation differences with a complex bearing von Willebrand disease mutations. *J Biol Chem* 279:23327–23334.
- [3] Emsley, J., M. Cruz, R. Handin, and R. Liddington, 1998. Crystal structure of the von Willebrand factor A1 domain and implications for the binding of platelet glycoprotein Ib. *J Biol Chem* 273:10396–10401.
- [4] Zhang, Q., Y.-F. Zhou, C.-Z. Zhang, X. Zhang, C. Lu, and T. A. Springer, 2009. Structural specializations of A2, a force-sensing domain in the ultralarge vascular protein von Willebrand factor. *Proc Natl Acad Sci USA* 106:9226–9231.
- [5] Matsui, T., K. Titani, and T. Mizuochi, 1992. Structures of the asparagine-linked oligosaccharide chains of human von Willebrand factor. Occurrence of blood group A, B, and H(O) structures. *J Biol Chem* 267:8723–8731.
- [6] Woods Group, 2005-2013. GLYCAM web. In: *Woods RJ, editor. Athens, GA: Complex Carbohydrate Research Center, The University of Georgia.* .
- [7] Schrödinger, LLC, 2010. The PyMOL molecular graphics system, version 1.3r1.
- [8] Van der Spoel, D., E. Lindahl, B. Hess, G. Groenhof, A. E. Mark, and H. J. C. Berendsen, 2005. GROMACS: fast, flexible, and free. *J Comput Chem* 26:1701–1718.
- [9] Hess, B., C. Kutzner, D. van der Spoel, and E. Lindahl, 2008. GROMACS 4: Algorithms for highly efficient, load-balanced, and scalable molecular simulation. *J Chem Theory Comput* 4:435–447.

- [10] Pronk, S., S. Pll, R. Schulz, P. Larsson, P. Bjelkmar, R. Apostolov, M. R. Shirts, J. C. Smith, P. M. Kasson, D. van der Spoel, B. Hess, and E. Lindahl, 2013. GROMACS 4.5: a high-throughput and highly parallel open source molecular simulation toolkit. *Bioinformatics* 29:845–854.
- [11] Schneidman-Duhovny, D., Y. Inbar, R. Nussinov, and H. J. Wolfson, 2005. Patchdock and Symmdock: servers for rigid and symmetric docking. *Nucleic Acids Res* 33:W363–W367.
- [12] Mashich, E., D. Schneidman-Duhovny, N. Andrusier, R. Nussinov, and H. J. Wolfson, 2008. Firedock: a web server for fast interaction refinement in molecular docking. *Nucleic Acids Res* 36:W229–W232.
- [13] Canis, K., T. A. J. McKinnon, A. Nowak, M. Panico, H. R. Morris, M. Laffan, and A. Dell, 2010. The plasma von Willebrand factor O-glycome comprises a surprising variety of structures including abh antigens and disialosyl motifs. *J Thromb Haemost* 8:137–145.
- [14] D. van der Spoel, B. H., E. Lindahl, and *et al.*, 2010. Gromacs User Manual version 4.5.6. www.gromacs.org.
- [15] Hornak, V., R. Abel, A. Okur, B. Strockbine, A. Roitberg, and C. Simmerling, 2006. Comparison of multiple amber force fields and development of improved protein backbone parameters. *Proteins: Struct Funct Bioinf* 65:712–725.
- [16] Best, R. B., and G. Hummer, 2009. Optimized molecular dynamics force fields applied to the helix-coil transition of polypeptides. *J Chem Phys B* 113:9004–9015.
- [17] Lindorff-Larsen, K., S. Piana, K. Palmo, P. Maragakis, J. L. Klepeis, R. O. Dror, and D. E. Shaw, 2010. Improved side-chain torsion potentials for the Amber ff99SB protein force field. *Proteins: Struct Funct Bioinf* 78:1950–1958.
- [18] Kirschner, K. N., A. B. Yongye, S. M. Tschampel, J. Gonzalez-Outeirio, C. R. Daniels, B. L. Foley, and R. J. Woods, 2008. GLYCAM06: a generalizable biomolecular force field. Carbohydrates. *J Comput Chem* 29:622–655.
- [19] Jorgensen, W. L., J. Chandrasekhar, J. D. Madura, R. W. Impey, and M. L. Klein, 1983. Comparison of simple potential functions for simulating liquid water. *J Chem Phys* 79:926–935.
- [20] Joung, I. S., and T. E. Cheatham, 2008. Determination of alkali and halide monovalent ion parameters for use in explicitly solvated biomolecular simulations. *J Chem Phys B* 112:9020–9041.
- [21] Hess, B., H. Bekker, H. J. C. Berendsen, and J. G. E. M. Fraaije, 1997. LINCS: A linear constraint solver for molecular simulations. *J Comput Chem* 18:1463–1472.
- [22] Feenstra, K. A., B. Hess, and H. J. C. Berendsen, 1999. Improving efficiency of large time-scale molecular dynamics simulations of hydrogen-rich systems. *J Comput Chem* 20:786–798.
- [23] Miyamoto, S., and P. A. Kollman, 1992. Settle: An analytical version of the SHAKE and RATTLE algorithm for rigid water models. *J Comput Chem* 13:952–962.
- [24] Hockney, R. W., and J. W. Eastwood, 1988. Computer simulation using particles. Bristol: Hilger.
- [25] Darden, T., D. York, and L. Pedersen, 1993. Particle mesh Ewald: An Nlog(N) method for Ewald sums in large systems. *J Chem Phys* 98:10089–10092.
- [26] Essmann, U., L. Perera, M. L. Berkowitz, T. Darden, H. Lee, and L. G. Pedersen, 1995. A smooth particle mesh Ewald method. *J Chem Phys* 103:8577–8593.
- [27] Bussi, G., D. Donadio, and M. Parrinello, 2007. Canonical sampling through velocity rescaling. *J Chem Phys* 126:014101 – 014101–7.

- [28] Berendsen, H. J. C., J. P. M. Postma, W. F. van Gunsteren, A. DiNola, and J. R. Haak, 1984. Molecular dynamics with coupling to an external bath. *J Chem Phys* 81:3684–3690.
- [29] Parrinello, M., and A. Rahman, 1981. Polymorphic transitions in single crystals: A new molecular dynamics method. *J Appl Phys* 52:7182–7190.
- [30] Connolly, M. L., 1983. Analytical molecular surface calculation. *J Appl. Crystallogr.* 16:548–558.
- [31] Amadei, A., A. B. M. Linssen, and H. J. C. Berendsen, 1993. Essential dynamics of proteins. *Proteins: Struct., Funct., Gen.* 17:412–425.
- [32] Lyskov, S., and J. J. Gray, 2008. The RosettaDock server for local protein-protein docking. *Nucleic Acids Res* 36:W233–W238.
- [33] Schneppenheim, R., J. J. Michiels, T. Obser, F. Oyen, A. Pieconka, S. Schneppenheim, K. Will, B. Zieger, and U. Budde, 2010. A cluster of mutations in the D3 domain of von Willebrand factor correlates with a distinct subgroup of von Willebrand disease: type 2A/IIIE. *Blood* 115:4894–4901.
- [34] Budde, U., R. Schneppenheim, J. Eikenboom, A. Goodeve, K. Will, E. Drewke, G. Castaman, F. Rodeghiero, A. B. Federici, J. Batlle, A. Prez, D. Meyer, C. Mazurier, J. Goudemand, J. Ingerslev, D. Habart, Z. Vorlova, L. Holmberg, S. Lethagen, J. Pasi, F. Hill, and I. Peake, 2008. Detailed von Willebrand factor multimer analysis in patients with von willebrand disease in the european study, molecular and clinical markers for the diagnosis and management of type 1 von willebrand disease (MCMDM-1VWD). *J Thromb Haemost* 6:762–771.
- [35] Budde, U., R. Schneppenheim, H. Plendl, J. Dent, Z. M. Ruggeri, and T. S. Zimmerman, 1990. Luminographic detection of von Willebrand factor multimers in agarose gels and on nitrocellulose membranes. *Thromb Haemost* 63:312–315.
- [36] Schneppenheim, R., H. Plendl, and U. Budde, 1988. Luminography—an alternative assay for detection of von Willebrand factor multimers. *Thromb Haemost* 60:133–136.
- [37] Crosslinkers and protocols for AFM Tip functionalization. Johannes Kepler University, Linz, Austria. March-October 2013. Web. 08 April 2015. <http://www.jku.at/biophysics/content/e257042> .
- [38] Hutter, J. L., and J. Bechhoefer, 1993. Calibration of atomic-force microscope tips. *Rev Sci Instrum* 64:1868–1873.
- [39] Ebner, A., P. Hinterdorfer, and H. J. Gruber, 2007. Comparison of different aminofunctionalization strategies for attachment of single antibodies to AFM cantilevers. *Ultramicroscopy* 107:922–927.
- [40] Zhu, R., S. Howorka, J. Prll, F. Kienberger, J. Preiner, J. Hesse, A. Ebner, V. P. Pastushenko, H. J. Gruber, and P. Hinterdorfer, 2010. Nanomechanical recognition measurements of individual dna molecules reveal epigenetic methylation patterns. *Nat Nanotechnol* 5:788–791.
- [41] RICKHAM, P. P., 1964. Human Experimentation: Code of Ethics of World Medical Association. DECLARATION OF HELSINKI. *Br Med J* 2:177.
- [42] Brehm, M. A., V. Huck, C. Aponte-Santamaría, T. Obser, S. Grässle, F. Oyen, U. Budde, S. Schneppenheim, C. Baldauf, F. Gräter, S. W. Schneider, and R. Schneppenheim, 2014. Von Willebrand disease type 2A phenotypes IIC, IID and IIE: A day in the life of shear-stressed mutant von Willebrand factor. *Thromb Haemost* 112:96–108.